coatings

MDPI

Article

Corrosion Protection of N80 Steel in Hydrochloric Acid Medium Using Mixed $C_{15}H_{15}NO$ and Na_2WO_4 Inhibitors

Jun Hu [1,2,*], Tiantian Wang [1], Zhen Wang [1], Liping Wei [1], Jianbo Zhu [1], Maosheng Zheng [1] and Zhong Chen [2,*]

1 School of Chemical Engineering, Northwest University, Xi'an 710069, China; m15529239355@163.com (T.W.); 18700404968@163.com (Z.W.); weiliping@nwu.edu.cn (L.W.); jianzhu@nwu.edu.cn (J.Z.); mszhengok@aliyun.com (M.Z.)

2 School of Materials Science and Engineering, Nanyang Technological University, 50 Nanyang Avenue, Singapore 639798, Singapore

* Correspondence: hujun@nwu.edu.cn (J.H.); ASZChen@ntu.edu.sg (Z.C.); Tel.: +86-029-8830-3216 (J.H.); +65-6790-4256 (Z.C.)

Received: 10 July 2018; Accepted: 3 September 2018; Published: 6 September 2018

Abstract: A novel inhibitor based on mixed Mannich base ($C_{15}H_{15}NO$) and Na_2WO_4 was developed for the corrosion prevention of N80 steel in hydrochloric acid solution. Infra-red spectrum, electrochemical measurements, X-ray Photoelectron Spectroscopy, and Scanning Electron Microscopy were used to understand the inhibition efficiency and mechanism. The results showed that the mixed inhibitors reduced the corrosion current density and increased the interface resistance. The inhibition efficiency is the highest when the ratio of $C_{15}H_{15}NO$ to Na_2WO_4 is 1:1 in the mixture. Observed from the surfaces, the number of pits and small cracks was reduced on the surface in the presence of the optimized inhibitors. The inhibition film can successfully hinder the chloride ions from reaching the bulk steel.

Keywords: corrosion inhibition; binding energy; N80 steel

1. Introduction

N80 steel is a commonly used material for pipelines for the petroleum and natural gas industry. This material suffers from serious corrosion problems when exposed to hydrochloric acid medium during industrial processes, such as acid cleaning, acid picking, acid descaling, and oil well acidizing [1–4].

In recent years, applying inhibitors has attracted a great deal of attention because of its advantageous properties, including its environmental friendliness, high efficiency, and convenience in application. Inhibitors can be divided into two types: organic and inorganic. Most inhibitors are organic compounds containing nitrogen, oxygen, or sulfur atoms [5–11]. It is generally believed that the organic molecules can produce a barrier layer through adsorption at the metal-solution interface [12,13], thus hindering the transfer of electrons between the metal substrate and the corrosion solution [14]. More and more researches have revealed that a single inhibitor has a limited effect, and mixed inhibitors are able to improve the protection effectiveness. For example, Meng et al. studied the inhibitor mechanism of Mannich base ($C_{15}H_{15}NO$) and Thiourea in a gas-field wastewater. The results showed that a bi-layer inhibitor film with an inner layer of Thiourea molecules and an outer layer of $C_{15}H_{15}NO$ displayed a greatly improved inhibition efficiency [15]. Shibli et al. discussed the co-inhibition characteristics of sodium tungstate (Na_2WO_4) with potassium iodate. It was concluded that the presence of an oxidizing agent like KIO_3 can enhance the inhibition of

tungstate [16]. Huang et al. [17] analyzed the inhibition performance of Na_2WO_4 and sodium lauroyl sarcosine for carbon steels in seawater. They revealed that the adsorption of sodium tungstate on the surface of carbon steel followed the Langmuir adsorption mechanism, and mixed inhibitors had a better corrosion performance than Na_2WO_4 alone [17]. Although both $C_{15}H_{15}NO$ and Na_2WO_4 have been used as corrosion inhibitors in hydrochloric acid, most of them were used alone or in combination with other substances. Until now, little attention has been devoted to the investigation of the inhibition effect of $C_{15}H_{15}NO$ with Na_2WO_4 for N80 steel in hydrochloric acid medium.

The objective of this paper is to discuss the inhibition mechanism of mixed $C_{15}H_{15}NO$ and Na_2WO_4 for N80 steel in an acidic medium. Optimization of the $C_{15}H_{15}NO$:Na_2WO_4 ratio was explored. Infra-red (IR) spectrum, electrochemical tests, X-ray photoelectron spectroscopy (XPS), and scanning electron microscopy (SEM) were used to assist in the understanding of the inhibition effectiveness and corrosion prevention mechanism.

2. Experimental Procedures

The chemical composition of N80 steel is shown in Table S1. The concentration of Na_2WO_4 (AR, $\geq$99.5%, Shanghai Sinopharm Group, Shanghai, China) is 0.0002 M. $C_{15}H_{15}NO$ was synthesized based on the conventional method [18]. The ratio of the $C_{15}H_{15}NO$ to Na_2WO_4 in the mixture was setting as 20:1, to 10:1, 2:1, 1.25:1, 1:1, and 0.67:1, respectively. Two types of specimens were used: one is the circular columns with dimensions of $\Phi 14.5 \times 5$ mm^2 for electrochemical measurements; the other is a cuboid block with dimensions of $5 \times 5 \times 3$ mm^3 for micrographic analysis. All specimens were manually polished by metallographic emery papers with a grit size from 400 to 800, 1000, and 1200. Afterward, they were immersed in petroleum ether for 10 min, washed thoroughly with distilled water, degreased with acetone, washed again with bidistilled water, and ultimately dried at room temperature [19].

The electrochemical experiments were conducted in a nitrogen environment, using the CS350 electrochemical workstation (Wuhan CorrTest Instruments Corp., Ltd., Wuhan, China) with a three-electrode system. The sweeping rate during polarization measurements was 0.5 mV·s^{-1}, and the potential was changed from –500 to +500 mV vs. E_{oc}. Electrochemical Impedance Spectroscopy (EIS) measurements were carried out at the open-circuit potential for alternating voltage amplitudes of 10 mV over a frequency range of 100 kHz to 10 mHz. The IR spectrum was recorded on a Perkin Elmer FTIR (PerkinElmer, Waltham, MA, USA) pls check instrument with a resolution of 4 cm^{-1}, and the aperture was set as 2.5 mm. XPS was taken by a Shimadzu-Kratos AXIS Ultra ^{DLD} (Kratos Analytical Ltd., Kyoto, Japan) which uses Al Kα as the excitation source, and operated in the constant 1486.7 eV analyzer energy mode with a pass energy of 50 eV. The sputtering speed was 2.4 nm s^{-1} and the angle between the sample and the ion gun was 30°. The accuracy of the reported binding energy is $\pm$0.1 eV. The C 1*s* peak at 284.6 eV, from adventitious carbon, was used as the reference for all spectra. Quantification of the atomic layer composition and the spectral simulation of the experimentally observed peaks were performed using Thermo Avantange software (V4.88) [20]. SEM images of N80 steel samples were taken by ZEISS SIGMA (ZEISS, Oberkochen, Germany). More details about the experimental procedures are available in section S1 of the Supporting Information.

The inhibition efficiency, η is calculated by:

$$\eta = \frac{I_{corr(0)} - I_{corr(i)}}{I_{corr(0)}} \quad (1)$$

where $I_{corr(0)}$ is the value of the corrosion current density before adding inhibitor molecules and $I_{corr(i)}$ is the value of the corrosion current density after adding the inhibitor. The surface coverage (θ) is an important parameter for the evaluation of the quality of the corrosion inhibitor film, and it can be calculated by:

$$\theta = 1 - \frac{R_{ct}^0}{R_{ct}} \quad (2)$$

where R_{ct}^{0} is the charge transfer resistance of the blank electrode and R_{ct} is the charge transfer resistance after adding the inhibitor to the solution.

3. Results and Discussion

3.1. IR Spectrum Analysis of $C_{15}H_{15}NO$

The IR spectrum of the prepared red-brown $C_{15}H_{15}NO$ liquid is shown in Figure 1.

The characteristic absorption peak of the synthesized product at 1402.21 cm^{-1} indicates the existence of the C–N bond. The strong characteristic absorption peak at 1688.66 cm^{-1} convincingly demonstrates the existence of carbonyl. The N–H stretching vibration absorption peak of secondary amine emerges at 3438.98 cm^{-1}, which infers the existence of the $C_{15}H_{15}NO$ structure in the synthesized product. The normal skeleton stretching vibration of the aromatic ring has four bands. They are respectively located at 1450, 1500, 1585, and 1600 cm^{-1}, which is one of the important signs to determine the presence of the benzene ring. Since there are peaks at 1449.83, 1508.36, 1582.49, and 1611.72 cm^{-1} corresponding to the above four bands from 1425 to 1650 cm^{-1}, the existence of the benzene ring in the synthetic product can be confirmed. Simultaneously, the C–H stretching vibration absorption peak of the benzene ring arises at 3095.66 cm^{-1}. Therefore, the synthesized red-brown liquid is $C_{15}H_{15}NO$ solution.

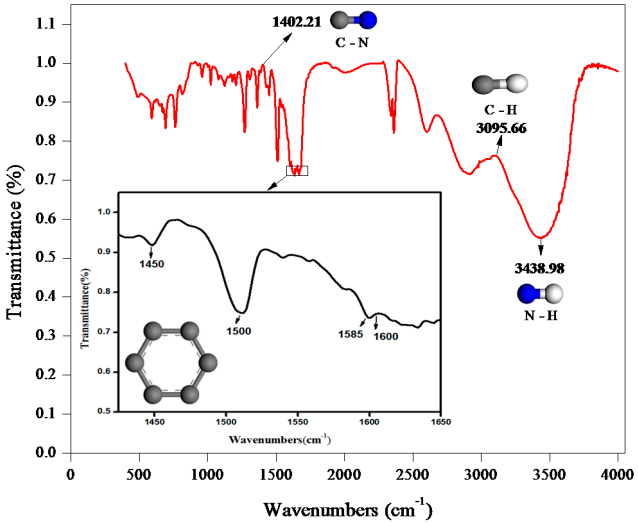

Figure 1. IR spectra of synthetic products.

3.2. Electrochemical Analysis

3.2.1. Potentiodynamic Polarization Studies

The potentiodynamic polarization curves for the N80 steel with different inhibitors are shown in Figure 2.

The corrosion current density is one of the significant indexes used to evaluate the corrosion resistance of the material. The greater the corrosion current density is, the more serious the corrosion of the material is [21]. From the polarization curve, it can be seen that the current density decreased after the inhibitors were added. The slope change of the anodic and cathodic poles indicates that the mixed inhibitors can hinder the anodic and cathodic reactions simultaneously, i.e., the compound inhibitor is a mixed-type inhibitor.

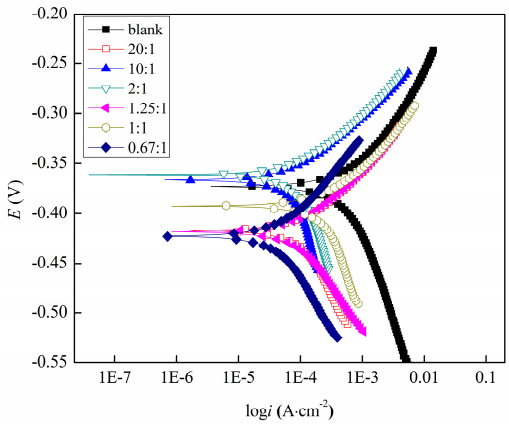

Figure 2. Polarization curves of N80 steel in the absence and presence of the inhibitor in 15% HCl solution at 60 °C under the environment of N_2 after 12 h immersion. Fitted polarization data are shown in Table S2.

3.2.2. EIS Studies

Nyquist and Bode plots acquired for the N80 steel electrode are shown in Figure 3.

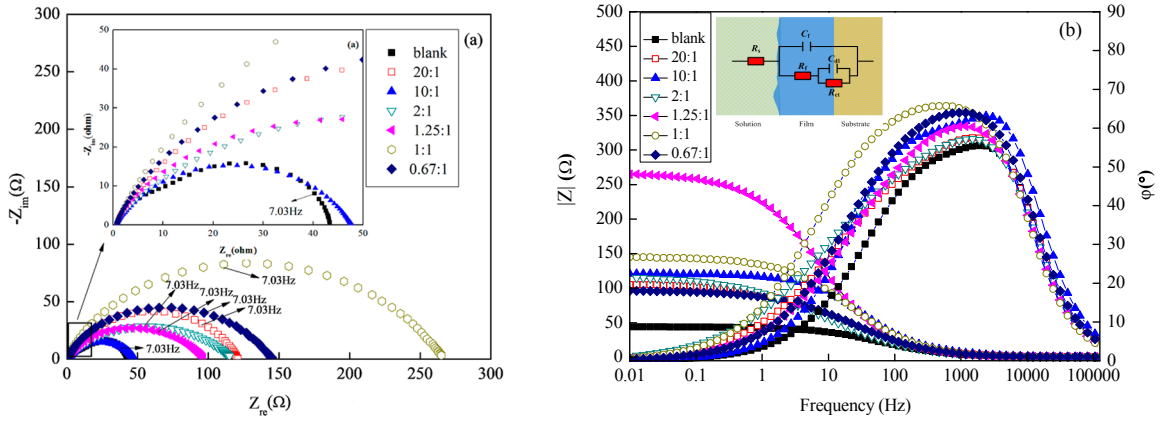

Figure 3. (**a**) Nyquist and (**b**) Bode diagram for N80 steel in the absence and presence of the inhibitor in 15% HCl solution at 60 °C under the environment of N_2 after 12 h immersion.

As shown in Figure 3a, the small radius of the capacitive arc for the blank sample indicates that the resistance of the corrosion reaction is small. This is mainly due to the corrosive Cl^- in the corrosion solution, which can easily diffuse through the metal-solution interface and cause damage to the surface of N80 steel [22,23]. Furthermore, each impedance spectrum is not a complete semicircle, which may be owing to the dispersion effect [24]. After adding mixed inhibitors with different ratios, the capacitance arc radius becomes larger. The large capacitive arc radius indicates that the corrosion inhibitor forms a protective film on the surface of N80 steel to increase the charge transfer resistance. The capacitive arc in the high-frequency region represents the characteristics of a metal surface film [25]. What is more, the maximum radius of the capacitive arc appears when the inhibitor ratio is 1:1, which shows that the corrosion process on the surface of N80 steel has been strongly restrained in this case. As shown in Figure 3b, the $|Z|$ versus log$f$ plot in the medium frequency range is an oblique line with a 45° slope, and the relative maximum phase angle in the Bode plots is smaller than 90°, which indicates that the system has good capacitance characteristics [26]. The R(Q(R(QR))) equivalent circuit diagram (with minimum error) is used in this paper, and the fitting data is shown in Table 1.

From Table 1, the charge transfer resistance, R_{ct}, changes after adding different concentrations of $C_{15}H_{15}NO$ and Na_2WO_4. The value of R_{ct} reflects the speed of the electrochemical reaction at the electrode solution interface [27,28]. When the metal surface is covered with the corrosion inhibitor

film, the barrier effect of the film on the charge transfer changes the impedance response of the electrode-solution interface. This increase of R_{ct} after adding mixed inhibitors is due to the enhanced capacitive arc radius in the high-frequency area and the decrease of the double-layer capacitance. Meanwhile, since the dielectric constant of organic molecules is smaller than that of water [29], the double-layer capacitance is smaller than that of the control electrode. Therefore, the corrosion inhibitor film acts as a barrier to hinder the diffusion of Cl^- from the solution to the metal surface, and slows down the rate of the corrosion reaction. The data in Table 1 reflect that the charge transfer resistance is the largest when the concentration ratio of $C_{15}H_{15}NO$ to Na_2WO_4 is 1:1 (the concentrations of $C_{15}H_{15}NO$ and Na_2WO_4 were both 0.0002 mol·L^{-1}). The result proves that the effect of mixed inhibitors is the best at the 1:1 concentration ratio. A comparison with other kinds of inhibitors is shown in Table S3. The cyclic voltammetry of N80 steel in mixed inhibitors proved that the corrosion inhibitor film structure is quite stable at different applied potentials (Figure S1). Figures S2 and S3 show that the mixed-inhibitor can greatly improve the performance and obeys the Langmuir adsorption isotherm on the N80 steel surface in the HCl solution. Based on the calculations, the highest value of θ is 0.849. Furthermore, θ has a good consistency with η, which was obtained from the polarization curve in Table S2.

Table 1. Electrochemical parameter of N80 steel obtained from the EIS Equivalent electrical circuit.

Sample/mol·L^{-1}			R_s/Ω·cm^2	C_f/S·s^n·cm^{-2}/×10^{-5}	n_1/0 < n < 1	R_f /Ω·cm^2	C_{dl}/S·s^n·cm^{-2}/*10^{-2}	n_2 /0 < n < 1	R_{ct}/Ω·cm^2	θ
HCl	$C_{15}H_{15}NO$	Na_2WO_4								
	0	0	0.6821	2.375	0.9656	4.102	0.057	0.6694	39.34	–
	0.004	0.0002	0.8403	1.833	0.8728	3.789	0.089	0.5647	102.1	0.615
	0.002	0.0002	0.7169	2.184	0.8899	3.064	0.046	0.6856	83.99	0.532
4.865	0.0004	0.0002	0.7487	2.177	0.9937	2.901	0.011	0.5495	114.8	0.657
	0.00025	0.0002	0.8093	2.169	0.8972	3.918	0.035	0.5889	92.24	0.574
	0.0002	0.0002	0.7571	2.484	0.9844	5.217	0.034	0.6518	260.9	0.849
	0.00013	0.0002	0.8079	1.89	0.9423	5.589	0.034	0.634	139.2	0.717

3.3. Analysis of Scanning Electron Microscopy

SEM images for N80 steel are shown in Figure 4. As indicated in Figure 4a, the morphology of the N80 steel sample without the inhibitors was damaged by corrosion with pits, cracks, and corrosion products observed on the surface of N80 steel. When separately applied, the inhibitor film of $C_{15}H_{15}NO$ was flaky without full coverage (Figure 4b), and the inhibitor film of Na_2WO_4 was layered and unevenly distributed (Figure 4c). However, the morphology of the N80 steel specimen in the mixed inhibitors was greatly improved. Figure 4d demonstrates a much improved corrosion resistance when the mixed inhibitors were used. Many particles appeared on the much smaller flaky structure, and the small cracks disappeared although there were still few pits on the surface. In summary, the combination of $C_{15}H_{15}NO$ and Na_2WO_4 can more effectively prevent the corrosion of N80 steel in 15% hydrochloric acid medium.

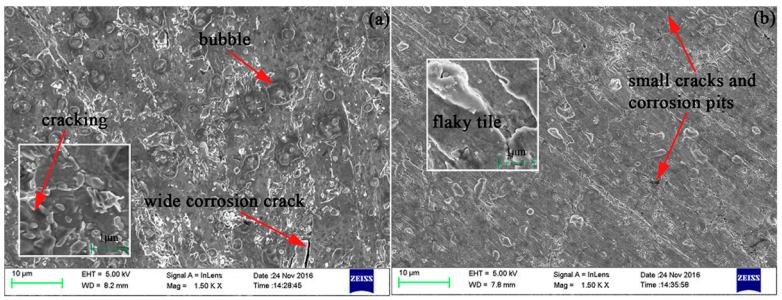

Figure 4. *Cont.*

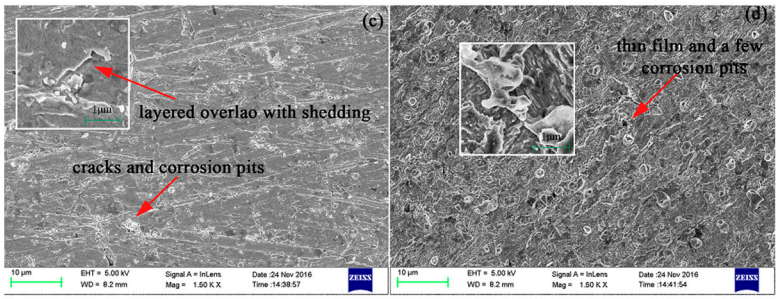

Figure 4. SEM image of N80 steel after 12 h immersion in 15% HCl solution having (**a**) no inhibitor, (**b**) 0.0002 mol·L^{-1} $C_{15}H_{15}NO$, (**c**) 0.0002 mol·L^{-1} Na_2WO_4, and (d) 0.0002 mol·L^{-1} $C_{15}H_{15}NO$ and 0.0002 mol·L^{-1} Na_2WO_4.

3.4. X-ray Photoelectron Spectroscopy

3.4.1. XPS Survey Spectra Studies

The XPS survey spectra of the N80 steel are shown in Figure 5.

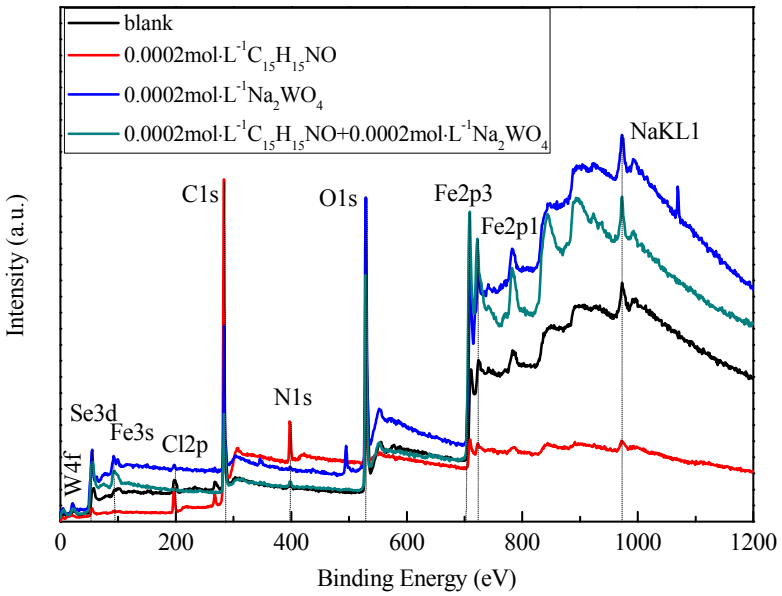

Figure 5. XPS survey spectra of the N80 steel in 15% HCl solution in the absence and presence of the inhibitor.

Figure 5 shows the presence of the O element from the external environment and Cl element from the corrosion solution, together with elements from the steel, in the absence of inhibitors. The elements on the surface of metal were mainly C, N, O, Fe, and Cl after adding the $C_{15}H_{15}NO$ [30]. The presence of N elements proves that $C_{15}H_{15}NO$ was adsorbed on the surface of N80 steel, while the peak of Cl elements indicates that the film of $C_{15}H_{15}NO$ only provides sufficient hindrance to the diffusion of Cl^-. Therefore, the N80 steel surface was still subject to serious corrosion with this single inhibitor. The precipitation film contained C, Fe, Se, Cl, O, N, and Na after adding the Na_2WO_4 inhibitors. The W, Na, and Fe element peaks reveal the fact that $FeWO_4$ has been deposited on the metal surface of N80 steel. Similarly, owing to defects of the $FeWO_4$ precipitation film on the metal surface, there was a significant Cl peak. The XPS survey spectra in mixed inhibitors show that the major elements of the surface of the membrane formed by the complex inhibitor were C, N, O, Fe, Se, W, and Na. In this case, no obvious Cl peak was detected, indicating that the corrosion product contains no or a very small amount of chloride. This indicates that the film formed can successfully prevent the chloride ions from entering and effectively improve the corrosion efficiency.

In comparison with the content of Cl at different ratios of $C_{15}H_{15}NO$ to Na_2WO_4 (Figure 6a), we find that the content of Cl will greatly change when the mixed ratio of the corrosion inhibitor changes. Furthermore, Cl was not detected when the ratio was 1:1, which indicates that this ratio is the most effective in corrosion prevention. The binding energy between Fe 2*p* and inhibitors, obtained by adsorption analysis, also verifies this conclusion (Table S4). Furthermore, the data with different plasma etch times (corresponding to different depths into the film) also indicate that mixed inhibitors can successfully hinder the Cl penetration, as shown in Figure 6b.

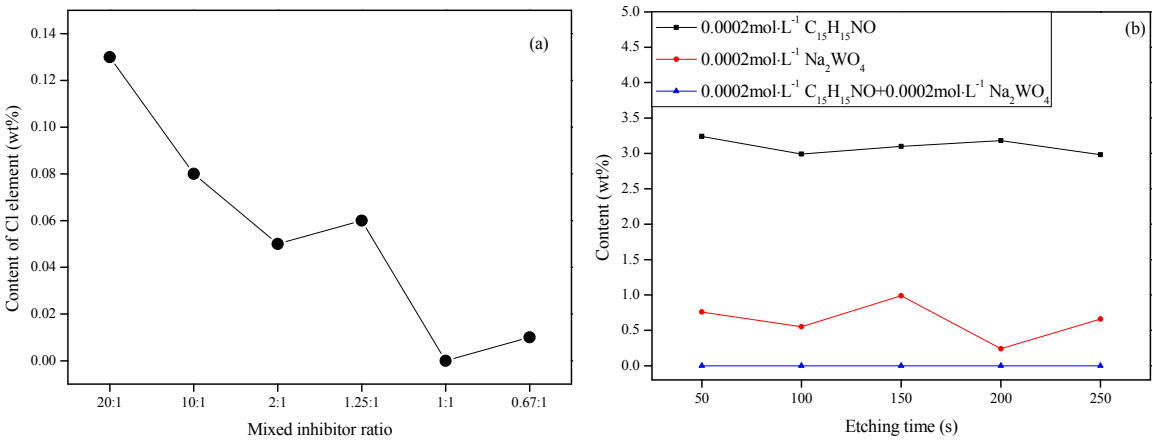

Figure 6. (**a**) Content of the Cl element on the N80 surface in different solutions. (**b**) Changes of C l2*p* content with etching time in corresponding corrosion solutions. Details of the XPS survey spectra can be found in Figure S4.

3.4.2. Analysis of Binding Energy of Film

The XPS survey spectrum and the spectrum of some elements on N80 steel in the mixed inhibitors with the ratio of 1:1 after a 250 s etching time are shown in Figure 7. In addition to the photoelectron spectra, the spectral lines of XPS also have satellite peaks, auger electron lines, spin orbit splitting (SOS), and ghost peaks [31].

As shown in Figure 7a, the C1s peak with a binding energy of 284.60 eV represents the C–C or C–H bond in the inhibitor molecule [32]. The peak from the N–H bond in the inhibitor molecule is located at 399.12 eV (Figure 7b), which is a strong evidence that the corrosion inhibitor molecules were adsorbed on the N80 steel surface [33]. In Figure 7c, binding energy at 528.98 eV is related to the dissolved oxygen in the etching solution, and the peak at 530.48 eV is ascribed to the C–O bond in the $C_{15}H_{15}NO$. According to the literature on XPS spectra of compounds containing different Fe valence values and the X-ray photoelectron spectroscopy manual, the Fe $2p_3$ peak of element Fe is at 706.75 eV, and the Fe2p3 peak of Fe_2O_3 is at 710.70 eV. Their corresponding Fe $2p_1$ peak spacing values are 13.2 and 13.6, which are at 719.45 eV and at 724.30 eV, respectively [34]. It can be inferred that in Figure 7d, the peaks between 706.52 eV and 719.52 eV come from elemental Fe, and the peaks between 709.228 eV and 722.62 eV belong to Fe_2O_3 formed by the reaction of elemental iron with oxygen on the surface of N80 steel [35–37]. The Na1s peak with a binding energy of 1072.94 eV in Figure 7e corresponds to Na^+ in the inhibitor molecule. Figure 7f is the Auger electron energy spectrum of Fe, whose kinetic energy has nothing to do with the incident light *hv*. The characteristic peaks located at 784 eV and 846.0 eV indicate the simultaneous existence of Fe(II) and Fe(III) on the surface of N80 steel [38,39]. Therefore, the protection film mainly consists of the inhibitor molecules and iron oxide or ferrous hydroxide.

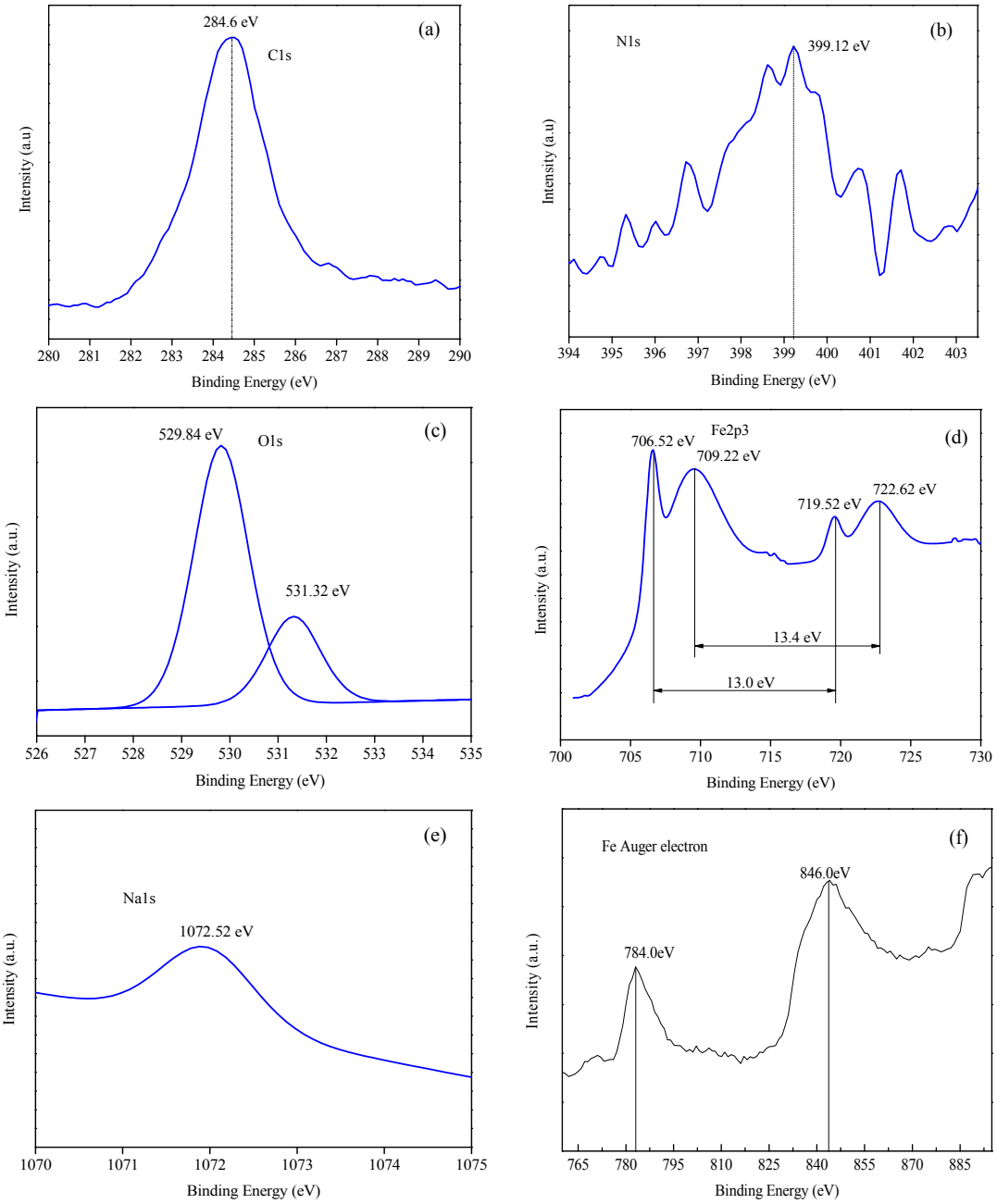

Figure 7. The XPS spectrum of some elements on N80 steel in the mixed inhibitors with the ratio of 1:1 for 250 s etching: (**a**) C 1*s* peak, (**b**) N 1*s* peak, (**c**) O 1*s* peak, (**d**) Fe 2*p* peak, (**e**) Na 1*s* peak, and (**f**) Fe Auger peak.

4. Conclusions

In this paper, the combined use of $C_{15}H_{15}NO$ and Na_2WO_4 as a corrosion inhibitor for N80 steel in 15% HCl solution was investigated by electrochemical experiments and microscopic analysis. The mixed inhibitors of Mannich base and sodium tungstate have demonstrated excellent corrosion prevention, and the best corrosion inhibition efficiency is 96.19% when the mixing ratio of the two components is 1:1. The SEM results indicate a fine and dense surface structure when the optimal mixed inhibitor was applied, and the degree of corrosion was greatly reduced compared with an un-protected surface or when a single inhibitor was used. The XPS analyses show that the content of Cl on the film was much decreased in the mixed inhibitor solution. The mixed inhibitors are able to form a stable membrane structure, which can effectively protect the metal from severe corrosion.

Supplementary Materials: The following are available online at http://www.mdpi.com/2079-6412/8/9/315/s1, Figure S1: Cyclic voltammetry of N80 steel at a mixed corrosion inhibitor ratio of 1:1 in 15% HCl solution at 60 °C under the environment of N_2, Figure S2: Degree of coverage for N80 steel in 15% HCl solution after adding the inhibitor at 60 °C under the environment of N_2, Figure S3: C/θ~C plots of different ratios of Mannich Base and Sodium Tungstate, Figure S4: (a) XPS survey spectra of 0.0002 mol·L^{-1} C15H15NO with etch time; (b) XPS survey spectra of 0.0002 mol·L^{-1} Na_2WO_4 with etch time; (c) XPS survey spectra of 0.0002 mol·L^{-1} C15H15NO and 0.0002 mol·L^{-1} Na_2WO_4 with etch time. Table S1: Chemical composition of N80, Table S2: Corrosion kinetics parameters of N80 steel with and without the inhibitor in 15% HCl solution at 60 °C under the environment of N_2, Table S3: The corrosion inhibition efficiency of different inhibitors in 15% HCl for N80 steel under the same experimental conditions in the literature, Table S4: Binding energy of Fe 2*p* on the surface of N80 steel under different inhibitors. References [40–47] are cited in the supplementary materials.

Author Contributions: Conceptualization, J.H. and Z.C.; Methodology, T.W. and Z.W.; Formal Analysis, L.W., J.Z. and M.Z.; Writing-Original Draft Preparation, T.W.; Writing-Review & Editing, J.H. and Z.C.; Funding Acquisition, J.H.

Funding: This research was funded by the National Natural Science Foundation of China (21676216, 51606153), China Postdoctoral Science Foundation (2014M550507, 2015T81046), and Innovative projects of Northwest University (YZZ17140).

Acknowledgments: Greatly acknowledgment to Xi'an Modern Chemistry Research Institute, who provided the experimental help.

Conflicts of Interest: The authors declare no conflict of interest.

References

1. Quraishi, M.A.; Sardar, R. Corrosion inhibition of mild steel in acid solutions by some aromatic oxadiazoles. *Mater. Chem. Phys.* **2003**, *78*, 425–431. [CrossRef]
2. El-Maksoud, S.A.; Fouda, A. Some pyridine derivatives as corrosion inhibitors for carbon steel in acidic medium. *Mater. Chem. Phys.* **2005**, *93*, 84–90. [CrossRef]
3. Migahed, M.; Nassar, I. Corrosion inhibition of tubing steel during acidization of oil and gas wells. *Electrochim. Acta* **2008**, *53*, 2877–2882. [CrossRef]
4. Finšgar, M.; Jackson, J. Application of corrosion inhibitors for steels in acidic media for the oil and gas industry: A review. *Corros. Sci.* **2014**, *86*, 17–41. [CrossRef]
5. Yadav, M.; Behera, D.; Sharma, U. Corrosion protection of N80 steel in hydrochloric acid by substituted amino acids. *Corros. Eng. Sci. Technol.* **2013**, *48*, 19–27. [CrossRef]
6. Yadav, M.; Sharma, U. Eco-friendly corrosion inhibitors for N80 steel in hydrochloric acid. *J. Mater. Environ. Sci.* **2011**, *2*, 407–414.
7. Kumar, S.; Sharma, D.; Yadav, P.N.; Yadav, M. Experimental and quantum chemical studies on corrosion inhibition effect of synthesized organic compounds on N80 steel in hydrochloric acid. *Ind. Eng. Chem. Res.* **2013**, *52*, 14019–14029. [CrossRef]
8. Vishwanatham, S.; Sinha, P. Corrosion protection of N80 steel in HCL by condensation products of aniline and phenol. *Anti-Corros. Methods Mater.* **2009**, *56*, 139–144. [CrossRef]
9. Emranuzzaman; Kumar, T.; Vishwanatham, S.; Udayabhanu, G. Synergistic effects of formaldehyde and alcoholic extract of plant leaves for protection of N80 steel in 15% HCL. *Corros. Eng. Sci. Technol.* **2004**, *39*, 327–332. [CrossRef]
10. Gardner, G.S.; Saukaitis, A.J. Inhibitor Acid. U.S. Patent 2,807,585, 2 December 1957.
11. Quraishi, M.A.; Ahamad, I.; Singh, A.K.; Shukla, S.K.; Lal, B.; Singh, V. *N*-(piperidinomethyl)-3-[(pyridylidene) amino]isatin: A new and effective acid corrosion inhibitor for mild steel. *Mater. Chem. Phys.* **2008**, *112*, 1035–1039. [CrossRef]
12. Olivares-Xometl, O.; Likhanova, N.; Domínguez-Aguilar, M.; Arce, E.; Dorantes, H.; Arellanes-Lozada, P. Synthesis and corrosion inhibition of α-amino acids alkylamides for mild steel in acidic environment. *Mater. Chem. Phys.* **2008**, *110*, 344–351. [CrossRef]
13. Quartarone, G.; Battilana, M.; Bonaldo, L.; Tortato, T. Investigation of the inhibition effect of indole-3-carboxylic acid on the copper corrosion in 0.5 M H_2SO_4. *Corros. Sci.* **2008**, *50*, 3467–3474. [CrossRef]
14. Ebenso, E.E.; Okafor, P.C.; Ekpe, U.J. Studies on the inhibition of aluminium corrosion by 2-acetylphenothiazine in chloroacetic acids. *Anti-Corros. Methods Mater.* **2003**, *50*, 414–421. [CrossRef]

15. Meng, F.N.; Li, Q.D.; Li, S.J. Synergistic inhibition mechanism of mannich bases and thiourea in corrosion system of gas-field wastewater. *Surf. Technol.* **2014**, *43*, 90–93.
16. Shibli, S.M.A.; Saji, V.S. Co-inhibition characteristics of sodium tungstate with potassium iodate on mild steel corrosion. *Corros. Sci.* **2005**, *47*, 2213–2224. [CrossRef]
17. Huang, L.; Xu, X.-E.; Wang, W.Q. Corrosion inhibition performances of sodium tungstate and its composite for carbon steel in simulated seawater. *Surf. Technol.* **2014**, *43*, 25–29. (In Chinese)
18. Ren, X.G.; Zhou, J.M.; Liu, D.; Li, L.; Song, Y.J. Corrosion inhibition of mannich base corrosion inhibitor to N80 steel. *Drill. Fluid Complet. Fluid* **2010**, *27*, 72–73. (In Chinese)
19. Hu, J.; Wang, Y.; Yu, L.J.; Zou, Y.Q.; Wang, Y.Q. An Investigation of a combined thiourea and hexamethylenetetramine as inhibitors for corrosion of N80 in 15% HCl solution: Electrochemical experiments and quantum chemical calculation. *Int. J. Corros.* **2015**, *2015*. [CrossRef]
20. El-Moneim, A.A.; Akiyama, E.; Habazaki, H.; Kawashima, A.; Asami, K.; Hashimotoetc, K. XPS and electrochemical studies on the corrosion behavior of sputter-deposited amorphous Mn-Nb alloys in a neutral chloride solution. *Corros. Sci.* **1998**, *40*, 1513–1531. [CrossRef]
21. Geler, E.; Azambuja, D.S. Corrosion inhibition of copper in chloride solutions by pyrazole. *Corros. Sci.* **2000**, *42*, 631–643. [CrossRef]
22. Epelboin, I.; Keddam, M.; Mattos, O.R.; Takenouti, H. The dissolution and passivation of Fe and Fe-Cr alloys in acidified sulphate medium: Influences of pH and Cr content. *Corros. Sci.* **1979**, *19*, 1105–1112. [CrossRef]
23. Epelboin, I.; Keddam, M. Kinetics of formation of primary and Secondary passivity in sulphuric aqueous media. *Electrochim. Acta* **1972**, *17*, 177–186. [CrossRef]
24. Ma, H.; Chen, S.; Niu, L.; Li, S.; Li, D. Inhibition of copper corrosion by several Schiff bases in aerated halide solutions. *J. Appl. Electrochem.* **2002**, *32*, 65–72. [CrossRef]
25. Gueshi, T.; Tokuda, K.; Matsuda, H. Voltammetry at partially covered electrodes: Part I. Chronopotentiometry and chronoamperometry at model electrodes. *J. Electroanal. Chem. Interfacial Electrochem.* **1978**, *89*, 247–260. [CrossRef]
26. Wang, Y.; Hu, J.; Wang, Y.Q.; Yu, L.J. A New Method for Preventing Corrosion Failure: Thiourea and Hexamethylenetetramine as Inhibitor for Copper. *Bull. Korean Chem. Sci.* **2016**, *37*, 1797–1811. [CrossRef]
27. Asawa, M.; Devasenapathi, A.; Fujisawa, M. Effect of corrosion product layer on SCC susceptibility of copper containing type 304 stainless steel in 1 M H_2SO_4. *Mater. Sci. Eng. A* **2004**, *366*, 292–298. [CrossRef]
28. Tüken, T.; Erbil, M. The use of polyindole for prevention of copper corrosion. *Surf. Coat. Technol.* **2006**, *200*, 4802–4809. [CrossRef]
29. Hu, S.Q.; Hu, J.C.; Fan, C.C.; Mi, S.Q.; Zhang, J.; Guo, W.Y. Corrosion inhibition of Q235 steel by a novel imidazoline compound under H_2S and CO_2 coexistence. *Acta Phys. Chimica Sin.* **2010**, *8*, 2163–2170.
30. Luo, H.; Su, H.Z.; Dong, C.F.; Xiao, K.; Li, X.G. Electrochemical and passivation behavior investigation of ferritic stainless steel in alkaline environment. *Constr. Build. Mater.* **2015**, *96*, 502–507. [CrossRef]
31. Zarrok, H.; Zarrouk, A.; Hammouti, B.; Salghi, R.; Jama, C.; Bentiss, F. Corrosion control of carbon steel in phosphoric acid by purpald–weight loss, electrochemical and XPS studies. *Corros. Sci.* **2012**, *64*, 243–252. [CrossRef]
32. Bouanis, M.; Tourabi, M.; Nyassi, A.; Zarrouk, A.; Jama, C.; Bentiss, F. Corrosion inhibition performance of 2,5-bis(4-dimethylaminophenyl)-1,3,4-oxadiazole for carbon steel in HCl solution: Gravimetric, electrochemical and XPS studies. *Appl. Surf. Sci.* **2016**, *389*, 952–966. [CrossRef]
33. Descostes, M.; Mercier, F.; Thromat, N.; Beaucaire, C.; Gautier-Soyer, M. Use of XPS in the determination of chemical environment and a data basis in binding energies for Fe and S reference compounds and applications to the evidence of surface species of an oxidized pyrite in a carbonate medium. *Appl. Surf. Sci.* **2000**, *165*, 288–302. [CrossRef]
34. Feng, Z.C.; Cheng, X.Q.; Dong, C.F.; Xu, L.; Li, X.G. Passivity of 316L stainless steel in borate buffer solution studied by Mott-Schottky analysis, atomic adsorption spectrometry and X-ray photoelectron spectroscopy. *Corros. Sci.* **2010**, *52*, 3646–3653. [CrossRef]
35. Devaux, R.; Vouagner, D.; De Becdelievre, A.M.; Duret-Thual, C. Electrochemical and surface studies of the ageing of passive layers grown on stainless steel in neutral chloride solution. *Corros. Sci.* **1994**, *36*, 171–186. [CrossRef]
36. Nakayama, N.; Obuchi, A. Inhibitory effects of 5-aminouracil on cathodic reactions of steels in saturated $Ca(OH)_2$ solutions. *Corros. Sci.* **2003**, *45*, 2075–2092. [CrossRef]

37. Pech-Canul, M.A.; Bartolo-Perez, P. Inhibition effects of *N*-phosphono-methyl-glyciney/Zn^{2+} mixtures on corrosion of steel in neutral chloride solutions. *Surf. Coat. Technol.* **2004**, *184*, 133–140. [CrossRef]
38. Galtayries, A.; Warocquier-Clérout, R.; Nagel, M.D.; Marcus, P. Fibronectin adsorption on Fe-Cr alloy studied by XPS. *Surf. Interface Anal.* **2006**, *38*, 186–190. [CrossRef]
39. Sastri, V.S.; Elboujdaini, M.; Rown, J.R.; Perumareddi, J.R. Surface analysis of inhibitor films formed in hydrogen sulfide medium. *Corrosion* **1996**, *52*, 447–452. [CrossRef]
40. Vishwanatham, S.; Haldar, N. Furfuryl alcohol as corrosion inhibitor for N80 steel in hydrochloric acid. *Corros. Sci.* **2008**, *50*, 2999–3004. [CrossRef]
41. Yadav, M.; Behera, D.; Sharma, U. Nontoxic corrosion inhibitors for N80 steel in hydrochloric acid. *Arab. J. Chem.* **2012**, *4*, 1487–1495.
42. Yadav, M.; Sharma, U.; Yadav, P.N. Isatin compounds as corrosion inhibitors for N80 steel in 15% HCl. *Egypt. J. Petroleum.* **2013**, *22*, 335–344. [CrossRef]
43. Zhou, Y.; Zuo, Y.; Lin, B. The compounded inhibition of sodium molybdate and benzotriazole on pitting corrosion of Q235 steel in NaCl + $NaHCO_3$ solution. *Mater. Chem. Phys.* **2017**, *192*, 86–93. [CrossRef]
44. Bokati, K.S.; Dehghanian, C.; Yari, S. Corrosion inhibition of copper, mild steel and galvanically coupled copper-mild steel in artificial sea water in presence of 1H-benzotriazole, sodium molybdate and sodium phosphate. *Corros. Sci.* **2017**, *126*, 272–285. [CrossRef]
45. Tremont, R.; Jesus-Cardona, H.D.; Garcia-Orozco, J. 3-Mercaptopropyltrimethoxysilane as a Cu corrosion inhibitor in KCl solution. *J. Appl. Electrochem.* **2000**, *30*, 737–743. [CrossRef]
46. Olivares, O.; Likhanova, N.V.; Gomez, B.; Navarrete, J.; Llanos-Serrano, M.E.; Arce, E.; Hallen, J.M. Electrochemical and XPS studies of decylamides of α-amino acids adsorption on carbon steel in acidic environment. *Appl. Surf. Sci.* **2006**, *252*, 2894–2909. [CrossRef]
47. Hosseini, M.; Mertens, S.F.L.; Arshadi, M.R. Synergism and antagonism in mild steel corrosion inhibition by sodium dodecylbenzenesulphonate and hexamethyleneteramine. *Corros. Sci.* **2003**, *45*, 1473–1489. [CrossRef]